JOURNAL OF GEOPHYSICAL RESEARCH, VOL. 106, NO. B12, PAGES 30,551–30,560, DECEMBER 10, 2001

Permeability reduction in granite under hydrothermal conditions

C. A. Morrow, D. E. Moore, and D. A. Lockner

U. S. Geological Survey, Menlo Park, California, USA

Abstract. The formation of impermeable fault seals between earthquake events is a feature of many models of earthquake generation, suggesting that earthquake recurrence may depend in part on the rate of permeability reduction of fault zone materials under hydrothermal conditions. In this study, permeability measurements were conducted on intact, fractured, and gouge-bearing Westerly granite at an effective pressure of 50 MPa and at temperatures from 150° to 500°C, simulating conditions in the earthquake-generating portions of fault zones. Pore fluids were cycled back and forth under a 2 MPa pressure differential for periods of up to 40 days. Permeability of the granite decreased with time t, following the exponential relation $k = c(10^{-rt})$. For intact samples run between 250° and 500°C the time constant for permeability decrease r was proportional to temperature and ranged between 0.001 and 0.1 days^{-1} (i.e., between 0.4 and 40 decades year^{-1} loss of permeability). Values of r for the lower-temperature experiments differed little from the 250°C runs. In contrast, prefractured samples showed higher rates of permeability decrease at a given temperature. The surfaces of the fractured samples showed evidence of dissolution and mineral growth that increased in abundance with both temperature and time. The experimentally grown mineral assemblages varied with temperature and were consistent with a rock-dominated hydrothermal system. As such mineral deposits progressively seal the fractured samples, their rates of permeability decrease approach the rates for intact rocks at the same temperature. These results place constraints on models of precipitation sealing and suggest that fault rocks may seal at a rate consistent with earthquake recurrence intervals of typical fault zones.

1. Introduction

Fluid flow within and around fault zones has a strong influence on stress state, frictional properties, and seismogenesis [*Hickman et al.*, 1995]. Many laboratory studies have investigated the permeability of intact, fractured, and comminuted rock at room temperature in order to quantify the effects of various physical parameters on fluid flow in fault zone materials [e.g., *Kranz et al.*, 1979; *Morrow et al.*, 1984, 1985]. However, studies at elevated temperatures are important for understanding earthquake processes because recent models of the earthquake cycle invoke the formation of low-permeability mineral seals within fault zones in the intervals between earthquakes [*Byerlee*, 1990; *Lockner and Byerlee*, 1995; *Miller et al.*, 1996]. These mineral seals may facilitate the development of high fluid pressure conditions within the fault zone, which is one of the explanations for the apparent weakness of the San Andreas fault that is implied by the lack of a measurable heat flow anomaly [*Brune et al.*, 1969; *Lachenbruch and Sass*, 1980].

Experimental studies of fault behavior under hydrothermal conditions are limited and do not always include direct permeability measurements [*Chester and Higgs*, 1992; *Blanpied et al.*, 1995; *Karner et al.*, 1997; *Nakatani*, 1998]. However, such studies are important not only for modeling fault zone behavior but also for understanding hydrothermal systems in general. *Moore et al.* [1994] measured the permeability of intact samples of Westerly granite in the temperature range 300°–500°C, simulating conditions near the base of the seismogenic zone. They found that the introduction of hydrothermal fluids to heated granite samples caused a reduction in permeability because of the healing and sealing of microfractures within the rock. In addition, the rate of permeability change increased with temperature. *Olsen et al.* [1998] observed permeability cycling during deformation experiments at elevated temperatures due to the formation and breaking of mineral seals. *Tenthorey et al.* [1998] and *Aharonov et al.* [1998] related permeability decreases to authigenic mineral formation during diagenesis experiments at elevated temperatures. All of these results support the fault valve model of ore deposit formation at the base of high-angle reverse faults [*Sibson*, 1992, 2001] and also the hypothesis that fault seals form in less time than the recurrence interval for large earthquakes at the base of the seismogenic zone.

In this paper, we continue the investigation of *Moore et al.* [1994] at lower temperatures of 150°–300°C, in the temperature range of interest for the seismogenic zone of the San Andreas Fault. These new permeability experiments show that fractured samples have higher rates of permeability reduction than intact samples, that mineral dissolution and precipitation rates are fast enough even at the lower temperatures of these experiments to produce significant changes in permeability over times of years to decades, and that the observed rates of permeability reduction are consistent with typical earthquake recurrence intervals along the San Andreas Fault.

2. Procedure

The sample configurations of the earlier study by *Moore et al.* [1994] (Table 1) simulated the following conditions in and around a fault zone [see, e.g., *Chester et al.*, 1993; *Caine et al.*, 1996]: the gouge-bearing fault core where seismic slip is

Paper number 2000JB000010.

concentrated (Figure 1a), the fractured damage-zone rock adjacent to the fault core (Figure 1b), and the undeformed country rock (Figure 1c). The fractured sample (400f) was produced by splitting the rock in tension along the cylindrical axis, and the gouge-bearing experiment (400g) used the <90 μm size fraction of crushed Westerly granite, which was then ground further in a ball mill to produce a rock flour. We report six new experiments in this study (Table 1), of which two are fractured samples (150f and 250f-1) and one an intact-rock sample (250i) identical in configuration to samples used by *Moore et al.* [1994]. The other three experiments utilize modifications of the basic sample configurations. The gouge-bearing experiment, 300g/f, used a layer of fine-grained quartz gouge sandwiched between fractured rather than intact granite pieces (Figure 1d). One fractured (250f-2) and one intact (150i) sample were made shorter in order to place coarse-grained, crushed-granite gouge (>0.71 mm sieve fraction) at either end (Figures 1e and 1f). Both sides of these gouge layers were held in place by stainless steel screen meshes. Unlike the other gouge-bearing experiments, the purpose of these gouge layers was to provide a heated fluid reservoir containing a large surface area of granitic material with which the fluid could interact before flowing into the rock. Because such a coarse gouge provides no resistance to flow, its volume was not included in the permeability calculations. The samples tested by *Moore et al.* [1994] and sample 250i of this study were 18.0 mm in diameter and 21.9 mm long. For the other five new experiments the total sample length was increased to 38.1 mm, and in addition, the samples were held together with a thin sleeve of teflon.

The sample column was jacketed in a copper sleeve and attached both to an end plug and to the loading piston of the triaxial apparatus. The end plug contained an inlet for the thermocouple and the pore fluid, connecting the high side to a small-volume fluid pump, and the piston contained an outlet for the pore fluid, connecting the low side to a larger-volume fluid pump. A furnace surrounded the sample assembly, providing a stable temperature along the axis of the sample.

All the permeability experiments were conducted at a confining pressure of 150 MPa and a pore pressure of 100 MPa for an effective pressure of 50 MPa, simulating a depth of ~ 3 km under hydrostatic fluid pressure conditions in a fault zone. First, confining pressure and axial load were increased simultaneously to prevent separation of the piston from the sample assembly. Because these pressures are the same, the sample is under essentially zero differential stress in this setup. Pore

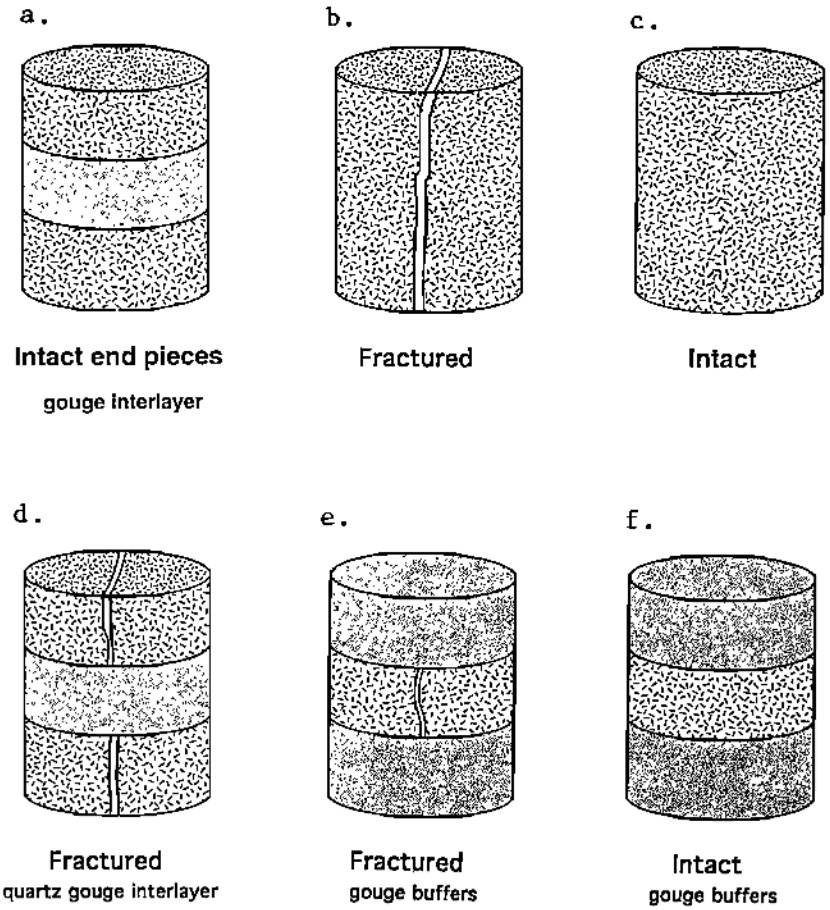

Figure 1. Cylindrical sample configurations for high-temperature permeability tests used in this study and by *Moore et al.* [1994] with experiment numbers from Table 1. (a) fine-grained gouge layer sandwiched between intact end pieces (400g); (b) cylinder split in tension (150f, 250f-1, and 400f); (c) intact granite cylinder (250i, 300i-1, 300i-2, 350i-1, 350i-2, 400i, 450i-1, 450i-2, 500i-1, and 500i-2); (d) crushed-quartz gouge layer sandwiched between fractured end pieces (300g/f); (e) sample fractured and surrounded by buffers of coarse-grained, crushed-granite gouge (250f-2); and (f) intact cylinder surrounded by buffers of coarse-grained, crushed-granite gouge (150i).

Table 1. Summary of experiments from this study and *Moore et al.* [1994][a].

Experiment Number	Sample Configuration	Temperature, °C	Number of Days Heated	k at Room T, $m^2 \times 10^{-21}$	k Heated, $m^2 \times 10^{-21}$ Initial	Final	$r \pm 2\sigma$ ($\times 10^{-3}$)	Decades Loss yr^{-1}
150i	intact, with granite gouge buffers	150	37.5	68	63.2	55.6	1.72 ± 0.40	0.63
150f	tensile fracture in granite	150	40.7	2918	3870.0	211.0	14.20 ± 2.90	5.18
250i	intact granite	250	35.6	86	61.3	29.3	2.00 ± 0.80	0.73
250f-1	tensile fracture in granite	250	28.0	89[b]	129.0	16.7	6.60 ± 1.70	2.41
250f-2	tensile fracture with granite gouge buffer	250	31 5	4870[b]	6900.0	980.0	11.37 ± 5.00	4.15
300g/f	quartz gouge, fractured granite end pieces	300	26.4	12817	15081.7	581.7	15.98 ± 0.40	5.83
300i-1	intact granite	300	19.5	413	166.1	59.1	8.10 ± 0.70	2.96
300i-2	intact granite	300	17 6	104	99.6	56.5	8.30 ± 1.02	3.03
350i-1	intact granite	350	13.6	473	171.5	92.0	3.41 ± 1.21	1.24
350i-2	intact granite	350	19.1	103	170.0	91.5	0.79 ± 0.82	0.29
400I	intact granite	400	45 8	193	137.6	18.3	19.08 ± 0.56	6.96
400f	tensile fracture in granite	400	27.8	14134	20864.0	31.4	---	---
400g	granite gouge, granite end pieces	400	23.7	876	1230.9	171.8	8.42 ± 0.55	3.07
450i-1	intact granite	450	19.5	1240	364.5	129.9	13.49 ± 0.33	4.92
450i-2	intact granite	450	20 0	466	404.0	121.4	14.50 ± 0.35	5.29
500i-1	intact granite	500	11.0	102	326.8	19.4	65.25 ± 16.95	23.81
500i-2	intact granite	500	9.8	609	465.4	0.4 ± 0.4	41.25 ± 3.93	15.06

[a] All were conducted at 150 MPa confining pressure and 100 MPa fluid pressure. Permeability loss rate r from $k = c(10^{-rt})$; also reported are the equivalent decades of permeability reduction per year.
[b] Average of final forward and reverse flow measurements.

pressure, provided by deionized water, was then applied. A pore pressure differential of 2 MPa was imposed between the top and bottom of the sample, producing a steady-state flow regime. Flow was reversed at intervals of 10,000-40,000s by reversing the 2 MPa fluid pressure gradient. In this way, the same volume of fluid flowed back and forth through the sample. The shorter intervals were used while permeabilities were changing rapidly.

The volume change of the small pore fluid reservoir was recorded at room temperature until permeability stabilized. The sample was then heated, and temperature was maintained for a period of up to 40 days. Permeability was calculated for each interval of flow according to Darcy's law:

$$Q/A = k/\mu\ (dP/dx), \tag{1}$$

where Q is volumetric flow rate, A is the cross-sectional area of the sample, k is permeability, μ is the dynamic viscosity of water at the temperature and pressure of the experiment, and dP/dx is the pore fluid pressure gradient across the sample. Flow rate through the heated sample is calculated from flow rate of the pore pressure pump at room temperature and assuming conservation of mass by

$$Q_T = Q_{25°}\ (V_T/V_{25°}), \tag{2}$$

where V is the specific volume of water and the subscript T denotes the temperature in degrees Celsius. Typical errors in relative permeability values are ±5-10%. The lower limit for permeability measurement of the system is 1×10^{-22} m^2. In this study, we report an average or apparent permeability for each sample on the basis of overall sample dimensions and ignoring differences in hydraulic conductivity between fractured and intact rock. Since we measure total flow and total pressure drop across the sample, partitioning of flow between rock matrix and the fracture would be model dependent. Furthermore, in the present study, we are primarily interested in relative changes of permeability in individual tests.

At the conclusion of experiment 250f-2, pore fluid was extracted from the sample column for chemical analysis. The fluid sample was immediately diluted, filtered, and analyzed for cations and silica, using an inductively coupled plasma (ICP) technique. Fluids could not be sampled during the experiments without adversely affecting the fluid pressure and chemistry. All of the samples were examined with a scanning electron microscope (SEM) with the exception of 300g/f. Element abundance was determined with an energy dispersive X-ray (EDX) spectrometer. Because the surfaces of the fractured samples display much clearer evidence of mineral reaction than the intact samples, they are the focus of the textural observations reported in this paper. A polished thin section was also prepared, cut perpendicular to the fracture surface. Compositions of the igneous minerals in Westerly granite along with some of the larger crystals that grew at 400°C were obtained with an electron microprobe. Natural and synthetic minerals were used both for initial standardization and as internal standards during this analysis.

3. Results

3.1. Permeability

Results for the six experiments are shown in Figure 2, with earlier intact-rock experiments at 300°C included in Figure 2c

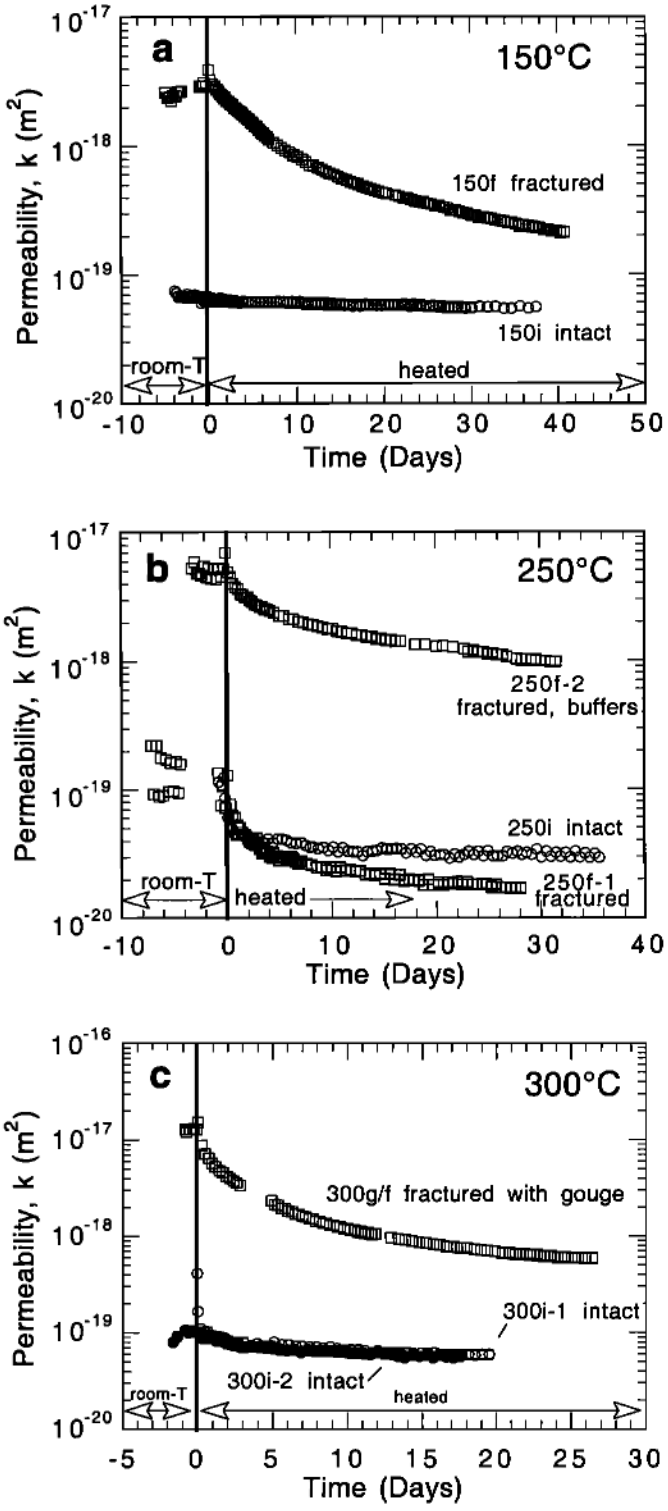

Figure 2. Permeability as a function of time for granite samples tested at (a) 150°C, intact (150i) and fractured (150f) samples; (b) 250°C, intact (250i), fractured (250f-1), and fractured with gouge buffers (250f-2); (c) 300°C, intact (300i-1 and 300i-2) and fractured with a quartz gouge layer (300g/f).

for comparison. The time $t = 0$ days is the time that a given sample reached the selected temperature of the experiment. In general, the initial heated permeabilities at $t = 0$ of the fractured samples were in the range 10^{-17} to 10^{-19} m^2, as much as 2 orders of magnitude higher than initial heated permeabilities for the intact samples, which fell between 10^{-19} and 10^{-20} m^2. The starting permeabilities for fractured samples are somewhat arbitrary because they depend in part on how well the two sample halves were remated. Fractured samples generally showed a greater rate of permeability decrease than intact samples. In most cases, permeability of the fractured samples appeared to reach a steady rate of decline on these log permeability plots toward the ends of the experiments.

At 150°C (Figure 2a) the intact sample showed little change in permeability with time, with a final value of 5.5×10^{-20} m^2. In contrast, the fractured sample exhibited a steady decline of permeability, beginning at a value almost 2 orders of magnitude higher than that of the intact sample and reaching a nearly constant rate of decline after ~ 30 days. The behavior was similar at 250°C (Figure 2b), although the permeability of the intact sample decreased rapidly during the first day after heating. Permeability of this sample approached a value of ~ 3×10^{-20} m^2, whereas the fractured samples continued to show steady declines after 20-30 days. Although the two 250°C fractured samples had different starting permeabilities, their trend of permeability loss was similar. (These two samples showed permeability oscillations between the forward and backward flow measurements at room temperature that are not an artifact of the test equipment. It is possible that there was some migration of debris during the flow reversals that could have affected the flow rate measurements). The 300°C results (Figure 2c) are similar in form to those at lower temperatures, with a large, smooth permeability decay in the fractured/gouge-bearing sample compared to more modest reductions in the two intact samples. The permeability loss for this sample closely resembles the three fractured-rock experiments shown in Figures 2a and 2b as well as the gouge-bearing sample tested at 400°C (400g, Table 1); [see also *Moore et al.*, 1994, Figure 3a]. Thus, although the flow paths of fluids through gouge-bearing and fractured rocks are undoubtedly different, the sample configurations cannot be distinguished by comparing the time response of permeability loss. The two intact-rock experiments at 300°C had nearly identical results, except for the first several hours following heating.

After the initial stage of rapid permeability loss, experiments generally reverted to a state in which permeability followed an exponential decay in time t, given by

$$k = c(10^{-rt}), \tag{3}$$

where permeability loss rate r (Table 1), was derived from the slope of the permeability curves. The calculated values of r exclude the first several days of the heated runs, which often decayed at a faster than exponential rate. While we recognize that assigning a fixed rate of decay to these relatively short term experiments using (3) may not completely describe the permeability behavior in some cases, this method has proven useful for comparing the diverse samples in this study. The permeability loss rates for the intact and fractured samples can be summarized by plotting r or, equivalently, decades loss per year versus temperature, as shown in Figure 3. Sample 300g/f is included with the fractured samples in Figure 3, and all of the intact-rock experiments from the earlier study are plotted. The r values for intact samples roughly correlate with temperature, whereas r values for the fractured samples appear to be independent of temperature. At a given temperature, the

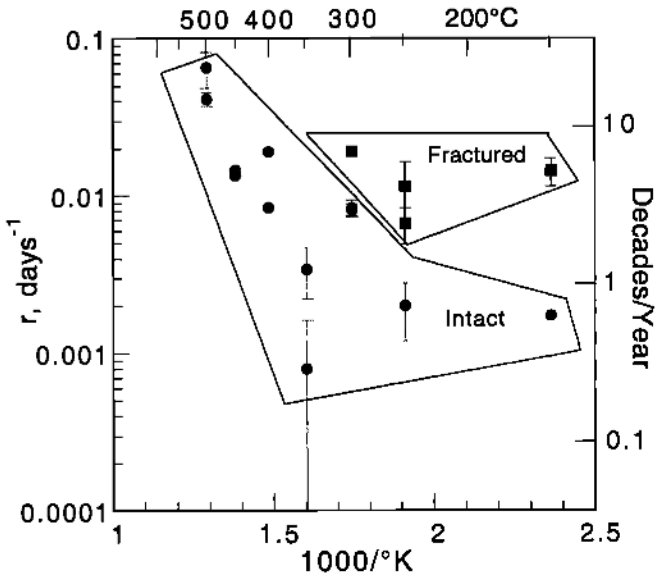

Figure 3. Permeability loss rate r from the equation $k = c(10^{-rt})$ versus temperature for fractured and intact samples of Westerly granite. Equivalent decades loss of permeability per year are shown on the right. Error is 2σ.

permeability loss rate is consistently higher for a fractured sample than for an intact sample.

3.2 Textural Observations

The Westerly starting material is a granodiorite that consists principally of plagioclase (~40 vol.%), K-feldspar (~25%), quartz (~25%), and biotite (~6%) [*Moore*, 1993]; the remainder is a variety of accessory igneous and secondary minerals (Table 2). Freshly fractured surfaces of Westerly display clean, smooth cleavage faces with sharp edges for the feldspars and biotite and smooth to rippled, conchoidally fractured surfaces of quartz. Particles of rock dust from the fracturing process adhere to the mineral surfaces.

When the samples were removed from their jackets for examination at the end of an experiment, the two sides of a fracture had to be forcefully separated, indicating induration or welding of fractures. The exposed fracture surfaces showed evidence of both mineral dissolution and crystallization that increased in abundance with temperature and with time. Dissolution features in quartz crystals include widened cracks and corroded surfaces; the faceted texture in Figure 4a suggests that certain crystallographic directions in the quartz were preferentially dissolved. Quartz was even more reactive at 400°C, and the preferential dissolution isolated many rounded fragments, creating piles of quartz debris on the fracture surface. At lower temperatures the feldspars showed pitted surfaces (Figure 4b) and etching along cleavage directions; at higher temperatures the etching was more pervasive and the corners of the crystals were rounded. These features all suggest a crystallographic control of dissolution process.

A wide variety of secondary minerals crystallized during the experiments (Table 2), including albite, K-feldspar, and quartz, which formed at all three temperatures. A few of the feldspars grew as isolated, euhedral crystals, but many of them occurred in mat-like clusters of crystals similar to the deposits in Figure 4a, whose flattened surfaces indicate that they spanned the fracture aperture. Some hydrothermal feldspars overgrow or partly replace the edges of igneous feldspar crystals (Figure 4c). Hydrothermal quartz crystals were somewhat less abundant than feldspar at all temperatures, and they usually but not exclusively grew on a quartz base. Sparry calcite crystals along with coatings (150° and 250°C) or fibrous filaments (400°C) of a phase rich in the rare earth elements cerium (Ce) and lanthanum (La) were also found at all three temperatures. The rare earth elements come from the alteration of accessory allanite (Table 2).

The most abundant mineral at 150° and 250°C was a phyllosilicate mineral that characteristically formed honeycomb

Table 2. Mineralogy of Samples[a].

Igneous Minerals	
Major Minerals:	plagioclase $Ab_{80}An_{20}$, K-feldspar Ab_8Or_{92}, quartz, biotite $K_2[Mg_{2.3}Fe_{2.6}][Al_{0.5}Ti_{0.3}][Al_{2.4}Si_{5.6}]O_{20}(OH)_4$
Accessory Minerals:	muscovite $[K_{1.9}Na_{0.1}]Mg_{0.2}[Fe_{0.7}Al_{3.1}][Al_{1.8}Si_{6.2}]O_{20}(OH)_4$, apatite, allanite, magnetite, ilmenite, titanite, zircon, pyrite, chalcopyrite.
Secondary Minerals:	chlorite: $[Mg_{4.5}Fe_{5.1}]Al_{2.4}[Al_{2.4}Si_{5.6}]O_{20}(OH)_{16}$, epidote $Ca_2[Fe_{0.8}Al_{2.2}]Al_2Si_3O_{12}(OH)$, clinozoisite: $Ca_2Al_3Si_3O_{12}(OH)$, muscovite, Albite: $Ab_{91}An_9$, titanite, calcite, TiO_2, fluorite.
Newly Crystallized Minerals, Fractured Samples	
150°C:	smectite (relatively Fe-rich), K-feldspar, albite, quartz, calcite, Ca-Al zeolite (laumontite?: $CaAl_2Si_4O_{12}{\cdot}4H_2O$), Ce-La coatings, traces of pyrite, barite
250°C:	smectite, calcite, K-feldspar, albite, quartz, Ca-Al zeolite (wairakite $CaAl_2Si_4O_{12}{\cdot}2H_2O$), Ce-La coatings; traces of K-mica, chlorite, and sphalerite; questionable apatite and titanite (latter may be loose relict grains)
400°C:	albite: $Ab_{96}An_1Or_3$, K-feldspar, pyroxene (ferrosilite: $Ca_{0.9}Na_{0.1}[Mg_{0.4}Fe_{0.5}]Al_{0.1}Si_2O_6$), Ca zeolite (xonotlite: $5CaSiO_3{\cdot}H_2O$?), quartz, calcite; traces of garnet (grossular. $[Ca_4Mg_{0.7}Fe_{1.3}][FeAl_3]Si_6O_{24}$), titanite, epidote: $Ca_2[Fe_{0.8}Al_{2.2}]Si_3O_{12}(OH)$.

[a] Fe grouped with Mg in the mineral formulas is ferrous; Fe grouped with Al is ferric. The compositions listed for laumontite and wairakite are their ideal formulas; the other compositions represent electron microprobe analyses of minerals in the samples.

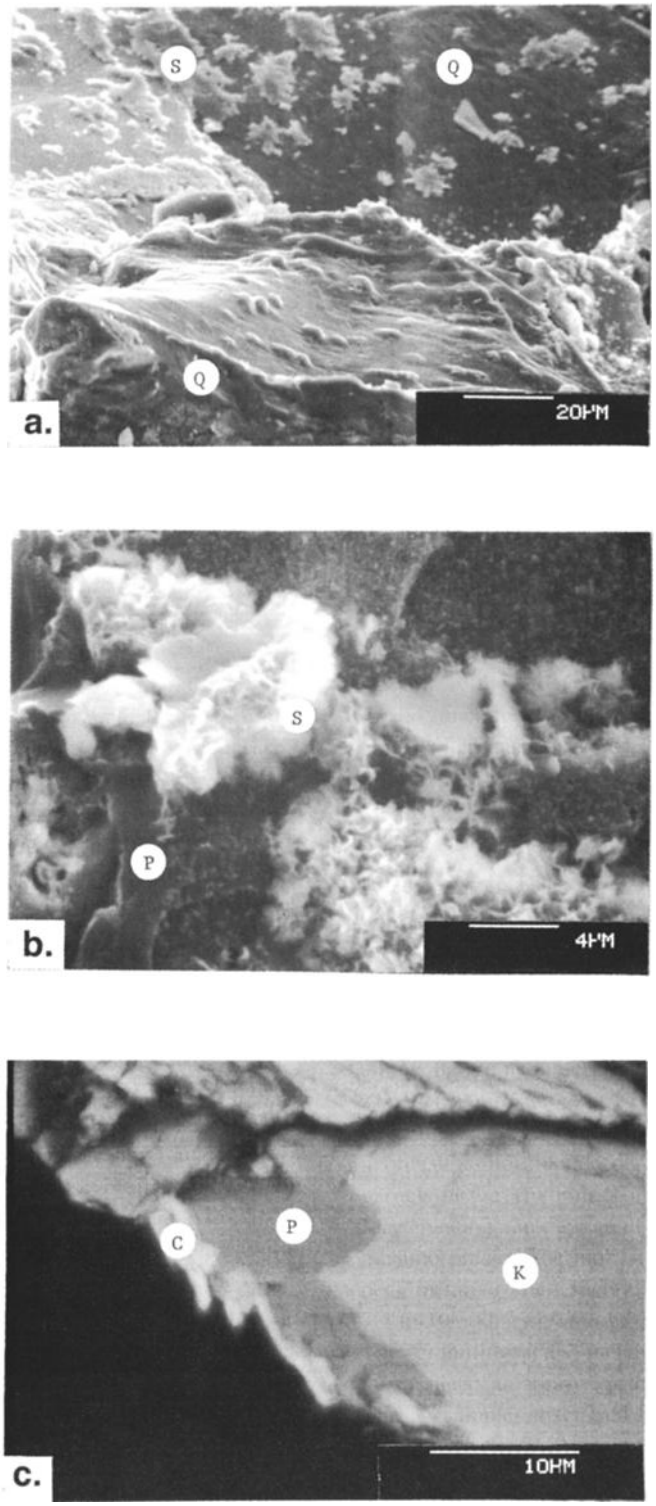

Figure 4. Scanning electron microscope photomicrographs of fractured samples. (a) Smectite (S) deposits on a corroded quartz (Q) crystal. The flattened surfaces of the smectite suggest that they grew against the opposing fracture wall. Secondary electron image of sample 150f. (b) Typical honeycomb character of smectite (S) deposits on a plagioclase (P) base. Partial dissolution of P is evident on the left. Secondary electron image of sample 250f-1. (c) Backscattered electron image of sample 250f-1. The texture of chlorite (C), intergrown with albitic plagioclase (P) at the tip of an igneous K-feldspar crystal, suggests that these crystals grew during the experiment. The growth pattern of P mimics the present fracture surface, indicating that it also formed during the experiment.

deposits (Figure 4b), whose habit corresponds to the smectite clays described by *Welton* [1984]. EDX spectra indicate the presence of Si, Al, Mg, Fe, and Ca, which is also consistent with smectite. Smectite element abundances vary considerably over a given fracture surface, but overall the clay appears to be more Fe-rich at 150°C than at 250°C. Minor amounts of a muscovitic K-mica and possibly of chlorite (Figure 4c) formed at 250°C. In contrast, the clinopyroxene mineral, ferrosilite, was one of the more abundant minerals to crystallize at 400°C, forming fibrous crystals or serrated blades. Bands of Fe-rich epidote, crystallized at 400°C in conjunction with calcite and the Ce-La-rich fibrous mineral, line pockets of void space alongside the fracture surface. In addition, a small number of grossular garnets crystallized at 400°C as partial replacements of chlorite. Clinopyroxene and garnet are high-temperature indicators in geothermal systems such as the one at Cerro Prieto, Mexico, where the clinopyroxene crystallized at temperatures ≥300°C and the garnet at ≥325°C [*Schiffman et al.*, 1985].

Possible zeolite minerals were present in all the fractured samples. Crystals rich in Ca, Al, and Si occurred as small, rounded blebs in the plagioclase crystals that line the fracture surfaces of the 150° and 250°C samples. Their EDX spectra indicate roughly the same cation proportions at both temperatures, and the relative peak heights of Al and Ca (compared to epidote) are consistent with the mineral laumontite (Table 2). On the basis of differences in crystal morphology, *Savage et al.* [1987] concluded that laumontite crystallized at 150°C and wairakite crystallized at 250°C during hydrothermal experiments on granitic rock. The compositions of laumontite and wairakite differ only in their H_2O contents; thus the same two minerals may have formed in these experiments. At 400°C a fibrous mineral containing roughly equal molar amounts of Ca and Si crystallized on plagioclase and quartz surfaces. The element proportions are suggestive of the zeolite mineral xonotlite ($5CaSiO_3 \cdot H_2O$), which *Frederickson and Cox* [1954] reported as a by-product of anorthite dissolution experiments at 350°C.

3.3 Fluid Chemistry

Silica (503 mg l^{-1}) and sodium (306 mg l^{-1}) predominate in the fluid sample collected at the end of experiment 250f-2 (Table 3), with lesser concentrations of calcium (22 mg l^{-1}), potassium (82 mg l^{-1}), and iron (19 mg l^{-1}). The measured silica concentration is close to the solubility of quartz at 250°C and 100 MPa fluid pressure (~560 mg l^{-1}) [e.g., *Morey et al.*, 1962; *Fournier and Potter*, 1982]. Application of the Na-K-Ca geothermometer of *Fournier and Truesdell* [1973] to the data in Table 3 also gives a temperature of 250°C.

Table 3. Partial analysis of fluid sample collected at the end of experiment 250f-2

species	mg l^{-1}
SiO_2	503
Na	306
K	82
Ca	22
Fe	19
Al	2.5
Mg	1.0

4. Discussion

4.1 Evaluation of Permeability Data

Two limitations of our experimental system could have an effect on the permeability results. First, to minimize corrosion of the pore fluid system, we used deionized water as the starting fluid rather than a fluid typical of natural geothermal waters. Deionized water could produce unrealistic permeability trends at the temperature and pressure conditions of the experiments, especially during the initial heating, when the fluid is in the greatest disequilibrium with the rock. Second, because the fluid pressure system is open from the room temperature reservoirs to the heated sample, dissolved species such as silica could potentially migrate away from the heated sample and be deposited in lower-temperature parts of the system, although we did not observe any evidence for this.

Our experimental design of flow through the granite cylinders mitigates part of the problem of starting fluid chemistry. Westerly granite contains saline pore fluids and/or salts deposited on mineral and crack surfaces, and water introduced into the samples will rapidly take up those salts. *Moore et al.* [1983] analyzed the compositions of two samples of initially deionized water that were flushed through cylinders of Westerly granite at room temperature during permeability investigations. The pore pressure system in those experiments was set up for one-way flow, and salt-bearing fluids were discharged from the granite cylinders over a period of a few days. The water contained bicarbonate, chloride, and sulfate ion as the principal anions, which are likely to be the major species in the starting fluid in the experiments of this study. Some of the bicarbonate and sulfate ion probably were removed from solution during the permeability experiments, as indicated by the crystallization of calcite and a scattering of sulfur-bearing minerals such as barite, pyrite, and sphalerite (Table 2). Chloride ion, however, can be considered a completely mobile component in hydrothermal fluids [e.g., *Giggenbach*, 1984] and because the pore pressure system of this study is a two-way, closed system, any chloride ion added to the water supply will remain there throughout the experiment. In turn, total cation concentrations must be high enough to balance the chloride and other anions that are present in the water. Some natural hydrothermal waters collected from felsic volcanic terrains are relatively dilute, nearly neutral chloride waters whose cation concentrations are similar to those in Table 3 [*Ellis and Mahon*, 1964; *Gunderson et al.*, 1995], which indicates that our sample water was representative of a natural hydrothermal fluid.

Dissolved silica is the one prominent component of hydrothermal fluids that is not abundant in the room temperature waters analyzed by *Moore et al.* [1983]. The two experiments with the gouge buffers (250f-2 and 150i) were designed in part to minimize the effect of such low initial dissolved silica concentrations. The buffers provide additional surface area with which the water can interact upon heating as well as serving as a reservoir for the small volume of water that was pushed back and forth through the sample during the permeability measurements. The gouge buffers also minimize the effect of any migration of species from the heated portion of the sample column to deposition sites at low temperatures. If some chemical migration did occur in our experiments, the gouge

buffers would be the immediate source of this material rather than the granite cylinders.

The trend of permeability decrease of the fractured sample containing gouge buffers (250f-2) is nearly identical to the fractured sample without gouge buffers (250f-1) (Figure 2b). Similarly, the permeability behavior of sample 150i (Figure 2a) is consistent with that of the other intact samples. This suggests that the data from experiments run without gouge buffers were not adversely affected either by the low initial silica contents of the fluids or by the temperature gradient in the pore pressure system.

4.2 Mechanisms of Permeability Change

Over the time span of the experiments the intact-rock samples behaved differently from the fractured and gouge-bearing samples (Figures 2 and 3). These differences were not a function of the initial permeabilities of the samples because samples 250i and 250f-1 had similar initial permeabilities but followed different paths of permeability reduction (Figure 2b). We propose that the rapid early permeability decreases in the fractured and gouge-bearing samples occurred in response to the enhanced dissolution of materials that the intact-rock samples largely lack. In fractured samples, preferentially dissolved material would include fine-grained particles generated while forming the tensile fracture, along with damaged areas and asperities on the fracture surface. In the gouge experiments the grinding process to produce a fine-grained gouge creates some ultrafine-grained material as well as damaged layers on the surfaces of the grains; some additional small particles are produced during the experiments as grains are crushed when the sample is pressurized. Ultrafine particles of minerals such as quartz have higher solubilities than the equilibrium solubilities for the minerals [*Morey et al.*, 1962], so that this material would be dissolved most rapidly. In addition, high-stress asperities may also be removed by pressure solution processes or by crushing. The removal of asperities will act to reduce crack width in addition to creating ultrafine material.

The preferred dissolution of fines, high surface energy damaged layers, and asperities may lead to supersaturated fluid environments in the immediate vicinity of the dissolving material that will be the preferred sites of mineral deposition. Such environments are particularly favorable for the growth of kinetically favored metastable minerals [*Dibble and Tiller*, 1981; *Potter et al.*, 1985], and some of the minerals deposited on the fracture surfaces may be examples of metastable crystallization. For example, at 400°C the zeolite mineral xonotlite is metastable relative to calcium-bearing minerals such as epidote and garnet, and at 250°C, K-mica + chlorite are typically the stable phyllosilicates in felsic rock types instead of smectite clays [e.g., *Browne*, 1978]. The formation of intermediate, metastable minerals is a common occurrence in geothermal systems [*Helgeson*, 1968; *Giggenbach*, 1981], such as those developed in glass-bearing volcanic rocks.

The very localized nature of the domains of supersaturation is also suggested by experiment 150i, in which the coarse-grained gouge buffers were external to the intact sample. This gouge lacked many of the high-solubility materials that are present in the gouge layers internal to the samples because the gouge was not ground to a powder. Even so, some enhanced dissolution may have occurred around grains that were crushed during pressurization of the sample. This supersaturation and accompanying mineral deposition would also be localized around the dissolving grains. Accordingly, the bulk fluid in the gouge-filled reservoir did not become supersaturated and did not cause enhanced mineral deposition in the intact rock sample.

As fines and asperities are progressively removed from the fractured and gouge-bearing samples, a thermodynamically stable mineral assemblage for the physical and chemical conditions of the experiments begins to form. Correspondingly, the rate of permeability reduction decreases toward the rate of the intact-rock experiment at the same temperature, where a stable system may be established within the first few days of the experiments. The experimental assembly replicates a rock-dominated hydrothermal system because of the closed fluid system and the low fluid/rock ratios. In the reaction-progress plots constructed by *Giggenbach* [1984] for such isochemical systems, the appearance of feldspars corresponds to the point where the solution becomes saturated with respect to thermodynamically stable assemblages involving all primary rock components. The relative timing of secondary mineral growth in the fractured samples could not be determined, but if the reaction-progress analysis of *Giggenbach* [1984] is applicable to these experiments, then the smectite clays that crystallized during experiment 250f-1 (Figure 4b) may be more representative of the initial stages of the experiment, and the albitic feldspar and chlorite (Figure 4c) may be more representative of the final days. The type of reaction illustrated in Figure 4c may also be characteristic of the intact-rock experiments. Permeability reductions accompanying such steady state reactions may occur in two major ways: first, through the rearrangement of minerals in the rock or a solution transport process, which may result in plugging of flow pathways, and second, through the replacement of the igneous mineral assemblage with a more hydrous, lower-temperature assemblage, which characteristically is accompanied by an increase in the volume of the solid phases.

In the time span of the experiments, none of the tensile-fracture surfaces became completely sealed with minerals, including sample 400f, whose final permeability was almost as low as that of 400i (Table 1). Some of the permeability reduction in the fractured samples can be attributed to the dissolution of asperities that propped the fracture open, which leads to a decrease in aperture width. The remaining permeability reduction may be caused by an increase in flow path tortuosity resulting from the scattered distribution of mineral deposits on the fracture surfaces (e.g., Figures 4a and 4c). The typical honeycomb growth pattern of the smectite clays may be especially effective in increasing tortuosity [*Welton*, 1984]. The strong influence of flow path tortuosity on permeability has been discussed in detail by *Tenthorey et al.* [1998] and *Aharonov et al.* [1998].

5. Application to Earthquake Environments

The formation of impermeable fault seals between earthquakes is a necessary condition in many models of earthquake generation [*Byerlee*, 1990; *Rice*, 1992; *Blanpied et al.*, 1995], where fault sealing combined with shear-induced compaction creates nearly lithostatic fluid pressures. The cyclic nature of the fault-sealing and fault-rupture process is discussed by *Sibson* [1992, 2001] in his "fault-valve" model of fault behavior and by *Chester et al.* [1993]. For these models to be realistic, impermeable seals must form in less

than the recurrence time of large earthquakes because the rupture process will begin the sealing and fluid-pressurization cycle anew. *Sieh et al.* [1989] proposed, on the basis of radiocarbon dating, that the recurrence interval at the site of 12 large earthquakes on the San Andreas Fault in southern California is between 50 and 300 years, with an average of ~132 years between major events. For a site in northern California, *Niemi and Hall* [1992] determined a recurrence interval of 221±40 years based on matching offset segments of a buried stream channel. Similarly, *Schwartz et al.* [1998] determined a 247–266 year recurrence interval for major earthquakes on the San Andreas Fault at a site in the Santa Cruz Mountains. Although these intervals vary widely between locations, they provide a rough upper limit of ~300 years between major events on the San Andreas with which to compare our fault sealing rates.

Experimentally determined rates of fault sealing are limited in number and have been addressed only for intact rocks by *Moore et al.* [1994]. They found that sealing rates at temperatures ≥400°C were sufficiently high (r = 0.01 to 0.1 days^{-1}; Table 1 and Figure 3) that the permeability of Westerly granite, around 10^{-19} m^2 at room temperature, could be expected to drop several orders of magnitude per year if the rates can be extrapolated to greater times. This suggests, along with diffusional crack healing studies in quartz [*Brantley et al.*, 1990; *Smith and Evans*, 1984], that microfractures at the base of the seismogenic zone will have geologically short lifetimes and that sealing rates are consistent with models of fault valve behavior and recurrence times of large earthquakes. The lower temperature results of *Moore et al.* [1994] were mixed, as permeability reduction at 350°C was lower than at 300°C. *Scholz et al.* [1995] also found that sealing rates were not strictly proportional to temperature at 200°–250°C. These observations notwithstanding, our new r values of 0.0008-0.008 days^{-1} (0.4-4.0 decades per year) for intact rocks from 150° to 350°C generally show a correlation with temperature that is consistent with the higher-temperature results (Figure 3), although the similarity between the 150°C and 350°C data suggest that the r–temperature relation may not be linear. Permeability reduction rates averaged one decade loss per year or less at the lower temperatures tested. Even these lower-temperature sealing rates could result in permeabilities that are low enough (<10^{-21} m^2) to restrict fluid flow through fault zones after only 10-20 years. More importantly, the fractured and gouge-bearing samples in the 150°–300°C temperature range have permeability reduction rates of several decades per year. Therefore fractured rocks will seal quickly even at the temperatures of the middle to shallow crust, so that their flow characteristics begin to resemble those of intact rocks with time. Permeability measurements of core samples from deep drillholes support this idea, as multiple episodes of hydrothermal healing and sealing of microfractures result in permeabilities as low as 10^{-23} m^2 [*Morrow et al.*, 1994], well below the level needed for the development of elevated fluid pressures [*Lachenbruch and Sass*, 1980].

The exponential decay of permeability (equation (3)) should be considered an empirical fit to the laboratory data. In fact, a power law relation of the form $k = a(t\text{-}b)^{-n}$ can also be used to model the experiments. While both exponential and power law forms will fit the existing data, they can lead to significantly different predictions for permeability loss rate when extrapolated to years or decades (the power law form predicts less of a permeability loss after many years). Given the practical limitations of carrying out long-term experiments, a better theoretical understanding of the processes controlling permeability loss would be helpful.

Many factors that affect sealing rates in the natural fault environment have not been addressed in this paper. These experiments were conducted at a fixed effective pressure with no differential stress in order to observe the effects of temperature and sample configuration on a granitic rock. However, microcracking will be enhanced in a differential stress environment, causing an increase in permeability, particularly under low effective confining pressure or as pore pressure increases toward the lithostatic load. In this case, the rate of permeability reduction will depend on the opposing mechanisms of permeability enhancement through microcracking and permeability reduction through hydrothermal deposition. The rate of permeability reduction will also vary with time around a seismically active fault because of the cycling of differential stress. In addition, differences in rock type or gouge composition may affect permeability changes under hydrothermal conditions. These considerations are all important when evaluating the permeability reduction rates that we have determined for the specific simulated fault environment in our experiments.

6. Conclusions

These new results provide a picture of permeability reduction rates in a hydrothermal environment for rock configurations representing intact country rock and the fractured and gouge-bearing portions of fault zones. Sealing rates r of intact granite scale with temperature in the range between 0.001 and 0.1 days^{-1}, which corresponds to ~ 0.4-40 decades per year decrease in permeability. At a given temperature, fractured samples consistently seal at a faster rate than intact samples, although with continued mineral reaction over time, the sealing rates as well as the permeability values should approach those of the intact rock. These sealing rates suggest that fault zones will become relatively impermeable in less time than the recurrence intervals of major earthquakes on faults such as the San Andreas. This finding is consistent with current models of earthquake generation in which faults undergo repeated cycles of mineral sealing, fluid pressurization, and rupture.

Acknowledgments. We thank Gil Ambats and Yousif Kharaka of the Water Resources Division, U. S. Geological Survey, for the analysis of the fluid sample.

References

Aharonov, E., E. Tenthorey, and C.H. Scholz, Precipitation sealing and diagenesis, 2, Theoretical analysis, *J. Geophys. Res.*, *103*, 23,969–23,981, 1998.

Blanpied, M.L., D.A. Lockner, and J.D. Byerlee, Frictional slip of granite at hydrothermal conditions, *J. Geophys. Res.*, *100*, 13,045–13,064, 1995.

Brantley, S.L., B. Evans, S.H. Hickman, and D.A. Crerar, Healing of microcracks in quartz: Implications for fluid flow, *Geology*, *18*, 136–139, 1990.

Browne, P.R.L., Hydrothermal alteration in active geothermal fields, *Annu. Rev. Earth Planet. Sci.*, *6*, 229–250, 1978.

Brune, J.N., T.L. Henyey, and R.F. Roy, Heat flow, stress, and rate of slip along the San Andreas fault, California, *J. Geophys. Res.*, *74*, 3821–3827, 1969.

Byerlee, J., Friction, overpressure, and fault normal compression, *Geophys. Res. Lett.*, *17*, 2109–2112, 1990.

Caine, J.S., J.P. Evans, , Forster, C.B., 1996. Fault zone architecture and permeability structure, Geology 24, 1025-1028.

Chester, F.M., and N.G. Higgs, Multimechanism friction constitutive model for ultrafine quartz gouge at hypocentral conditions, *J. Geophys. Res.*, *97*, 1859–1870, 1992.

Chester, F.M., J.P. Evans, and R.L. Biegel, Internal structure and weakening mechanisms of the San Andreas fault, *J. Geophys. Res.*, *98*, 771–786, 1993.

Dibble, W.E., Jr., and W.A. Tiller, Kinetic model of zeolite paragenesis in tuffaceous sediments, *Clays Clay Miner.*, *29*, 323–330, 1981.

Ellis, A.J., and W.A.J. Mahon, Natural hydrothermal systems and experimental hot-water/rock interactions, *Geochim. Cosmochim. Acta*, *28*, 1323–1357, 1964.

Fournier, R.O., and R.W. Potter, II, An equation correcting the solubility of quartz in water from 25° to 900°C at pressures up to 10,000 bars, *Geochim. Cosmochim. Acta*, *46*, 1969–1973, 1982.

Fournier, R.O., and A.H. Truesdell, An empirical Na-K-Ca geothermometer for natural waters, *Geochim. Cosmochim. Acta*, *37*, 1255–1275, 1973.

Frederickson, A.F., and J.E. Cox, Jr., The decomposition products of anorthite attacked by pure water at elevated temperatures and pressure, in *Proc. Second Nat. Conf. Clays Clay Minerals, Nat. Res. Council Publ.*, *327*, 111–119, 1954.

Giggenbach, W.F., Geothermal mineral equilibria, *Geochim. Cosmochim. Acta*, *45*, 393–410, 1981.

Giggenbach, W.F., Mass transfer in hydrothermal alteration systems – A conceptual approach, *Geochim. Cosmochim. Acta*, *48*, 2693–2711, 1984.

Gunderson, R.P., P.F. Dobson, W.D. Sharp, R. Pudjianto, and A. Hasibuan, Geology and thermal features of the Sarulla Contract Area, North Sumatra, Indonesia, in *Proceedings of the World Geothermal Congress*, 2, pp. 687–692, 1995.

Helgeson, H.C., Evaluation of irreversible reactions in geochemical processes involving minerals and aqueous solutions, I, Thermodynamic relations, *Geochim. Cosmochim. Acta*, *32*, 853–877, 1968.

Hickman, S., R. Sibson, and R. Bruhn, Introduction to special section: Mechanical involvement of fluids in faulting, *J. Geophys. Res.*, *100*, 12,831–12,840, 1995.

Karner, S.L., C. Marone, and B. Evans, Laboratory study of fault healing and lithification in simulated fault gouge under hydrothermal conditions, *Tectonophysics*, *277*, 41–55, 1997.

Kranz, R.L., A.D. Frankel, T. Engelder, and C.H. Scholz, The permeability of whole and jointed Barre granite, *Int. J. Rock Mech. Min. Sci. & Geomech. Abs.*, *16*, 225–234, 1979.

Lachenbruch, A.H., and J.H. Sass, Heat flow and energetics of the San Andreas fault zone, *J. Geophys. Res.*, *85*, 6185–6223, 1980.

Lockner, D.A., and J.D. Byerlee, An earthquake instability model based on faults containing high fluid-pressure compartments, *Pure Appl. Geophys.*, *145*, 717-745, 1995.

Miller, S.A., A. Nur, and D.L. Olgaard, Earthquakes as a coupled shear stress-high pore pressure dynamical system, *Geophy. Res. Lett.*, *23*, 197-200, 1996.

Moore, D.E., Microcrack populations associated with a propagating shear fracture in granite, *U.S. Geol. Surv. Open File Rep.*, *93-245*, 88 pp., 1993.

Moore, D.E., C.A. Morrow, and J.D. Byerlee, Chemical reactions accompanying fluid flow through granite held in a temperature gradient, *Geochim. Cosmochim. Acta*, *47*, 445–453, 1983.

Moore, D.E., D.A. Lockner, and J.D. Byerlee, Reduction of permeability in granite at elevated temperatures, *Science*, *265*. 1558–1561, 1994.

Morey, G.W., R.O. Fournier, and J.J. Rowe, The solubility of quartz in water in the temperature interval from 25° to 300°C, *Geochim. Cosmochim. Acta*, *26*, 1029–1043, 1962.

Morrow, C.A., D.E. Moore, and J.D. Byerlee, Permeability and pore-fluid chemistry of the Topopah Spring Member of the Paintbrush Tuff, Nevada Test Site, in a temperature gradient—Application to nuclear waste storage, *Mater. Res. Soc. Symp. Proc.*, *26*, 883–890, 1984.

Morrow, C.A., D.E. Moore, and J.D. Byerlee, Permeability changes in crystalline rocks due to temperature: Effects of mineral assemblage, *Mater. Res. Soc. Symp. Proc.*, *44*, 467–474, 1985.

Morrow, C., D. Lockner, S. Hickman, M. Rusanov, and T. Röckel, Effects of lithology and depth on the permeability of core samples from the Kola and KTB drill holes, *J. Geophys. Res.*, *99*, 7263–7274, 1994.

Nakatani, M., A new mechanism of slip weakening and strength recovery of friction associated with the mechanical consolidation of gouge, *J. Geophy. Res.*, *103*, 27,239-27,256, 1998.

Neimi, T.M., and N.T. Hall, Late Holocene slip rate and recurrence of great earthquakes on the San Andreas fault in northern California, *Geology*, *20*, 195–198, 1992.

Olsen, M.P., C.H. Scholz, and A. Léger, Healing and sealing of a simulated fault gouge under hydrothermal conditions: Implications for fault healing, *J. Geophys. Res.*, *103*, 7421–7430, 1998.

Potter, J.M., D.C. Pohl, R.N. Guillemette, H.B. Ponader, and J.G. Liou, A system for flow through experimental studies at hydrothermal conditions, *Neues Jahrb. Mineral. Monatsh.*, 329–335, 1985.

Rice, J.R., Fault stress states, pore pressure distributions, and the weakness of the San Andreas fault, in *Fault Mechanics and Transport Properties of Rock*, edited by B. Evans and T.-F. Wong, pp. 475–503, Academic, San Diego, Calif., 1992.

Savage, D., M.R. Cave, A.E. Milodowski, and I. George, Hydrothermal alteration of granite by meteoric fluid: An example from the Carnmenellis granite, United Kingdom, *Contrib. Mineral. Petrol.*, *96*, 391–405, 1987.

Schiffman, P., D.K. Bird, and W.A. Elders, Hydrothermal mineralogy of calcareous sandstones from the Colorado River delta in the Cerro Prieto geothermal system, Baja California, Mexico, *Mineral. Mag.*, *49*, 435–449, 1985.

Scholz, C.H., A. Léger, and S.L. Karner, Experimental diagenesis: Exploratory results, *Geophys. Res. Lett.*, *22*, 719–722, 1995.

Schwartz, D., D. Pantosti, K. Okumura, T. Powers, and J. Hamilton, Paleoseismic investigations in the Santa Cruz mountains, California: Implications for recurrence of large-magnitude earthquakes on the San Andreas fault, *J. Geophys. Res.*, *103*, 17,985–18,001, 1998.

Sibson, R.H., Implications of fault-valve behavior for rupture nucleation and recurrence, *Tectonophysics*, *211*, 283–293, 1992.

Sibson, R.H., Geology of the crustal earthquake source, in *International Handbook of Earthquake and Engineering Seismology*, edited by Lee, Kanamori, and Jennings, Academic, San Diego, Calif., 2001.

Sieh, K., M. Stuiver, and D. Brillinger, A more precise chronology of earthquakes produced by the San Andreas fault in southern California, *J. Geophys. Res.*, *94*, 603–623, 1989.

Smith, D.L., and B. Evans, Diffusional crack healing in quartz, *J. Geophys. Res.*, *89*, 4125–4135, 1984.

Tenthorey, E., C.H. Scholz, E. Aharonov, and A. Léger, Precipitation sealing and diagenesis, 1, Experimental results, *J. Geophys. Res.*, *103*, 23,951–23,967, 1998.

Welton, J.E., *SEM Petrology Atlas, Methods in Explor. Ser.*, 237 pp., Am. Assoc. Pet. Geol., Tulsa Okla., 1984.

D.A. Lockner, D.E. Moore, and C.A. Morrow, U.S. Geological Survey, 345 Middlefield Road, Mail Stop 977, Menlo Park, CA 94025, U.S.A. (cmorrow@usgs.gov)

(Received October 17, 2000; revised June 24, 2001;
accepted June 25, 2001.)